

Mass evaluation for red giant stars based on the spectroscopically determined atmospheric parameters

Yoichi Takeda¹

Abstract The mass (M) of a star can be evaluated from its spectroscopically determined effective temperature (T_{eff}) and metallicity ($[\text{Fe}/\text{H}]$) along with the luminosity (L ; derived from parallax), while comparing them with grids of theoretical evolutionary tracks. It has been argued, however, that such a track-based mass (M_{trk}) may tend to be overestimated for the case of red giants. Meanwhile, there is an alternative approach of evaluating mass (M_{gLT}) directly from surface gravity (g), L , and T_{eff} . The practical reliability of M_{gLT} was examined for ~ 100 benchmark giants in the *Kepler* field, for which atmospheric parameters are already determined and the reliable mass (M_{seis}) along with the evolutionary status are known from asteroseismology. In addition, similar check was also made for the accuracy of M_{trk} for comparison. It turned out that, while a reasonable correlation is seen between M_{gLT} and M_{seis} almost irrespective of the stellar property, its precision is rather insufficient because $\log(M_{gLT}/M_{\text{seis}})$ distributes rather widely within $\sim \pm 0.2$ – 0.3 dex. In contrast, the reliability of M_{trk} was found to depend on the evolutionary status. Although M_{trk} and M_{seis} are satisfactorily consistent with each other (typical dispersion of $\log(M_{\text{trk}}/M_{\text{seis}})$ is within $\sim \pm 0.1$ dex) for H-burning red giants as well as He-burning 2nd clump giants of higher mass, M_{trk} tends to be considerably overestimated as compared to M_{seis} by up to $\lesssim 0.4$ dex for He-burning 1st clump giants of lower mass. Accordingly, M_{gLT} and M_{trk} are complementary with each other in terms of their characteristic merit and demerit.

Keywords stars: atmospheres – stars: evolution – stars: fundamental parameters – stars: late-type

1 Introduction

1.1 Mass determination with evolutionary tracks

The mass (M) of a star is of decisive importance in astrophysics, because it essentially governs the stellar properties and their variations during the lifetime. The conventional method for determining this key parameter is to compare the position on the theoretical Hertzsprung–Russell (HR) diagram, where the bolometric luminosity of a star (L ; determinable from the observed brightness along with the distance) is plotted against its effective temperature (T_{eff}), with a set of stellar evolutionary tracks. Since these theoretical tracks (loci on the L vs. T_{eff} plane) are computed for various combinations of M and metallicity (z ; often regarded as equivalent to the Fe abundance $[\text{Fe}/\text{H}]$ in practice), M can be reasonably determined by finding the best-match between $(L, T_{\text{eff}})_{\text{obs}}$, and $(L, T_{\text{eff}})_{\text{cal}}^{\{M, z\}}$, if L , T_{eff} , and $[\text{Fe}/\text{H}]$ (z) are given as input observational parameters. Such established M is referred to as M_{trk} (track-based mass) in this paper.

This mass-evaluation technique is occasionally called “spectroscopic method” (despite that it is essentially based on theoretical stellar evolution calculations), because the use of spectroscopically determined T_{eff} and $[\text{Fe}/\text{H}]$ is almost prerequisite (since sufficient precision can not be attained by other simpler method such as the photometric one, especially for $[\text{Fe}/\text{H}]$). The widely adopted approach to accomplish this spectroscopic preconditioning is to make use of a number of Fe I and Fe II lines, by which T_{eff} , $\log g$ (surface gravity), v_t (microturbulence), and $[\text{Fe}/\text{H}]$ can be effectively established by the requirements of (i) excitation equilibrium of Fe I (abundances do not depend upon the excitation potential), (ii) ionisation equilibrium between Fe I and Fe II (equality of the mean abundances), and curve-of-growth matching for Fe I (abundances do not depend

Yoichi Takeda

¹11-2 Enomachi, Naka-ku, Hiroshima-shi 730-0851, Japan
E-mail: ytakeda@js2.so-net.ne.jp

upon the line strength) (see, e.g., Takeda, Ohkubo & Sadakane, 2002).

1.2 Suspicion on M_{trk} for red giants

However, the credibility of M_{trk} evaluated in this way for red giants (evolved stars with typical masses of $\sim 1.5\text{--}3 M_{\odot}$) has become a controversial issue. The background is that the importance of reliable mass determination for such cool giant stars has grown these days, especially with regard to the research field of extrasolar planets. Namely, since searching planets for such intermediate-mass stars is not easy when they are hot stars on the upper main sequence, those in the evolved red-giant stage (sometimes called “retired A-type stars” as done by Johnson et al., 2007) are more suitable and thus mainly targeted. As such, knowing the mass of the host giant is of critical importance, because it is one of the key parameters (like metallicity) affecting the physical properties and formation process of planets (e.g., Ghezzi, Montet, & Johnson, 2018; Wolthoff et al., 2022).

The doubt for the reliability of M_{trk} emerged almost a decade ago, when the novel approach of precise mass determination for red giants became possible by using the asteroseismic method based on very high-precision photometric observations from satellites (CoRoT, *Kepler*, TESS). That is, the track-based M_{trk} tends to be systematically larger compared to the seismologically established mass (M_{seis}), which suggests that the former would have been more or less overestimated. As a matter of fact, this possible overestimation of M_{trk} has been reported and argued in quite a few number of studies; e.g., Lloyd (2011, 2013); Schlaufman & Winn (2013); Johnson et al. (2014); Sousa et al. (2015); Ghezzi & Johnson (2015); Takeda & Tajitsu (2015); Takeda et al. (2016); Hjørringgaard et al. (2017); Stello et al. (2017); North et al. (2017); Campante et al. (2017); White et al. (2018); Ghezzi, Montet, & Johnson (2018); Malla et al. (2020); Wolthoff et al. (2022).

It is not clear, however, M_{trk} results for red giants of which type are seriously affected by errors or they may alternatively be regarded as practically usable, because the conclusions in these papers are rather diversified (some authors state that spectroscopic M_{trk} determination using grids of evolutionary tracks is not significantly affected by systematic errors and thus valid; e.g., Ghezzi & Johnson, 2015). In any event, we should be aware of the possibility that M_{trk} derived for giant stars may suffer appreciable errors, owing to the increasing difficulty of its application to red giants due to closely-lying (or even crossing) evolutionary tracks of different masses.

1.3 Mass derivation from surface gravity

Incidentally, there is another way of mass determination, which may also be called as “spectroscopic method” (like the case of M_{trk}) because it is similarly based on the spectroscopically established atmospheric parameters (T_{eff} and $\log g$) along with L (from the parallax). The point is to make use of the information of M contained in the surface gravity (g). That is, combining the two relations, $g \propto M/R^2$ (R : radius) and $L \propto T_{\text{eff}}^4 R^2$, we obtain $M \propto gL/T_{\text{eff}}^4$, or

$$\begin{aligned} \log(M/M_{\odot}) &= \log(g/g_{\odot}) \\ &+ \log(L/L_{\odot}) - 4 \log(T_{\text{eff}}/T_{\text{eff}\odot}). \end{aligned} \quad (1)$$

The mass determined from g , L , and T_{eff} by Eq. (1) is hereinafter referred to as M_{gLT} . Although this is a simple and straightforward approach without any necessity of using theoretical models (evolutionary tracks), it seems to have barely been employed in practice to the author’s knowledge for giants (though sometimes discussed for the case of dwarfs; e.g., Valenti, & Fischer, 2005). This is presumably because accomplishing sufficient precision in spectroscopic $\log g$ has been considered as rather difficult, especially for giant stars of lower density atmospheres. Actually, comparisons of the spectroscopically determined $\log g$ values for red giants in various literature suggest that they show an appreciable diversity (see, e.g., Fig. 5b, Fig. 6b, Fig. 7b, and Fig. 8b in Takeda, Sato & Murata, 2008; hereinafter referred to as T08), which indicates that $\log g$ determination is not robust but depends on technical details.

However, the author has come to think that spectroscopic $\log g$ may be relied upon based on the results of Takeda & Tajitsu (2015; hereinafter called as T15) and Takeda et al. (2016: T16), in which spectroscopically determined $\log g$ values of ~ 100 red giants in the *Kepler* field and those established by the seismological technique were compared and found to be in satisfactory agreement with each other (see Fig. A1 in T16).¹ Therefore, considering that the parallax data necessary for evaluation of L (many of which were unknown at the time of T15 and T16) are now available for all of the sample stars thanks to the *Gaia* DR2 database (Gaia Collaboration et al., 2016, 2018), it is interesting and worthwhile to examine whether and how the M_{gLT} values of these *Kepler* giants (derived from Eq. (1) by using

¹In the case of FGK-type main sequence stars, Brewer et al. (2015) arrived at a similar conclusion that their results of spectroscopic $\log g$ are in reasonable consistency with seismic gravities.

the atmospheric parameters already determined spectroscopically in T15 and T16) are compared with the seismic ones (M_{seis}). This is the main purpose of this study.

Besides, by taking this opportunity, the problem on the reliability of M_{trk} is revisited for these ~ 100 red giant stars. Since Ghezzi & Johnson (2015) concluded that M_{trk} values of their 59 benchmark giant stars derived by the open software PARAM² (da Silva et al., 2006), which is based on the Bayesian estimation method, are reasonably consistent with the reference mass values (derived either from orbital motions of binaries or by the seismic method), we likewise make use of the PARAM code to evaluate M_{trk} for our sample stars in the *Kepler* field, for which not only the mass but also the evolutionary status is seismologically established. Do we obtain a consistency between M_{trk} and M_{seis} ? Is there any dependence upon the evolutionary stage? To check these points is the second aim of this investigation.

2 Program stars

The main targets in this investigation are the 103 red giants in the *Kepler* field studied in T15 and T16 based on the high-dispersion spectra, most³ of which were obtained on 2014 September 9 and 2015 July 3 (UT) by using the High-Dispersion Spectrograph (HDS) of the Subaru Telescope. Their atmospheric parameters (T_{eff} , $\log g$, [Fe/H], and v_t) were determined from the equivalent widths of Fe I and Fe II lines by using the TGVIT⁴ program (Takeda et al., 2005), which is the update version of the TGV code (Takeda et al., 2002). The seismic mass values (M_{seis} ; to be used as the comparison reference) are the same as those adopted in T15 and T16, which were derived from the spectroscopic T_{eff} along with the seismological frequencies (ν_{max} and $\Delta\nu$; taken from Mosser et al., 2012) according to Eq. (2) of T15. Likewise, the evolutionary status (RG or RC1 or RC2; cf. the caption of Fig. 3) of each star is already determined by Mosser et al. (2012)

In addition, for the purpose of comparison with Ghezzi & Johnson’s (2015) results, 11 nearby field giants were also included, which are common to their 59

benchmark stars (cf. their Table 1) and whose atmospheric parameters are already determined in the previous papers of the author by using the TGVIT program. The M_{seis} values of 9 stars were calculated as in T15 by using ν_{max} and $\Delta\nu$ given in their Table 1, while (exceptionally) the reference masses of the components of Capella system (cooler primary and hotter secondary) are the results of Torres et al.’s (2015) orbital motion analysis. A total of 114 (=103+11) program stars and their stellar parameters are presented in Table 1.

3 Evaluation of luminosity

The luminosity L , another necessary parameter along with T_{eff} and $\log g$ in Eq.(1), is related with V (apparent visual magnitude in mag), π (parallax in milliarc-second) by the following equation

$$-2.5 \log(L/L_{\odot}) = V + 5 + \log(\pi/1000) - A_V + \text{BC} - 4.75, \quad (2)$$

where A_V is the interstellar extinction (in mag), BC is the bolometric correction (in mag), and 4.75 (mag) is the bolometric absolute magnitude of the Sun.

The V data of the program stars were obtained by consulting the SIMBAD database wherever possible. However, since the relevant data were unavailable for 13 *Kepler* giants, their apparent visual magnitudes were tentatively derived from the r -band magnitude (r^{KIC}) given in the *Kepler* Input Catalogue (Brown et al. 2011; hereinafter abbreviated as KIC) by the following procedure.

- First, for each *Kepler* giant with known V_{simbad} , theoretical $(V - R)_{\text{cal}}$ colour index corresponding to T_{eff} and $\log g$ is evaluated by using Girardi et al.’s (2000) grids of stellar evolution calculations.
- Then, this $(V - R)_{\text{cal}}$ is applied to r^{KIC} to derive v by the relation $v = (r^{\text{KIC}} - A_r^{\text{KIC}}) + (V - R)_{\text{cal}} + A_V^{\text{KIC}}$, where A_V^{KIC} is the interstellar extinction given in KIC and $A_r^{\text{KIC}} = 0.88A_V^{\text{KIC}}$ (cf. Brown et al., 2011).
- Such obtained v is plotted against V_{simbad} in Fig. 1a, which shows that the relation between these two is can be approximately expressed as $v = 0.934V + 1.002$.
- Accordingly, since v' (corrected v) defined by the relation $v' \equiv (v - 1.002)/0.934$ is nearly equivalent to V (almost free from systematic deviation; cf. Fig. 1b), this v' is adopted as V for each of the 13 *Kepler* giants for which V data are not available in SIMBAD.

The parallaxes (π) of all 114 program stars were taken from the SIMBAD database, which are mostly

²http://stev.oapd.inaf.it/cgi-bin/param_1.3/

³The spectra for 13 (out of 103) stars were taken from Thygesen et al. (2012). Regarding 3 stars (KIC 1726211, KIC 2714397, KIC 3744043) for which both Subaru data and Thygesen et al.’s (2002) data are available, the results based on the former Subaru spectra are adopted in this study.

⁴<https://www2.nao.ac.jp/~takedayi/tgv/>

from *Gaia* DR2 and of sufficient precision (errors are a few percent or less).⁵

The bolometric correction (BC) for each star was evaluated from T_{eff} and $[\text{Fe}/\text{H}]$ by using Eq.(17) and Eq.(18) (both results were averaged at the overlapping T_{eff} range) of Alonso, Arribas, & Martínez-Roger (1999).

Since the relevant red giants in the *Kepler* field are rather distant (distances up to ~ 2 kpc) and of low galactic latitude (typically $b \sim 10$ deg), they suffer appreciable interstellar extinction (A_V), for which two data sources were examined: (i) application of the EX-TINCT⁶ program (Hakkila et al., 1997) which yields averaged A_V and its error (based on various different extinction studies) if the data of distance and galactic coordinates are given, and (ii) A_V data given in KIC. These two kinds of A_V and the difference between them are plotted against the distance in Figs. 2a–2c. While we can see from these figures that both are mostly consistent with each other, A_V^{EXTINCT} is prominently larger than A_V^{KIC} for 10 stars deviating from the mean trend (cf. Fig. 2a). However, these anomalous A_V^{EXTINCT} values are questionable, because the corresponding L values obtained by Eq.(2) tend to become more discrepant in comparison with L_{seis} derived in T16 (from spectroscopic T_{eff} and seismic R) as shown in Figs. 2d and 2e. Therefore, we decided to adopt A_V^{KIC} wherever possible. A_V^{EXTINCT} values were employed only for 9 *Kepler* giants (for which A_V^{KIC} are not available) and for the additional 11 nearby giants.

The adopted data of V , A_V , π , and BC along with the resulting $\log L$ from Eq.(2) are summarised in Table 1, where the M_{gLT} values derived from Eq.(1) are also given. Besides, more complete data (including errors and data sources for V or A_V) are presented in the electronic data table (“stellar_parameters.dat”) available as the online material.

Now that T_{eff} and L have been established for all of the 114 stars, their locations in the $\log L$ vs. $\log T_{\text{eff}}$ diagram are plotted in Fig. 3 (RG, RC1, and RC2 are discriminated by different symbols in the same manner as in T16), where the theoretical PARSEC tracks (Bressan et al., 2012, 2013) corresponding to $z = 0.01$ are also drawn for comparison.

4 Mass from evolutionary tracks

In addition to such derived M_{gLT} , the track-based mass (M_{trk}) was also determined for all the sample stars.

Since the main motivation for doing this was to check Ghezzi & Johnson’s (2015) conclusion supporting the practical validity of M_{trk} (without any significant errors) derived for red giants, the open software tool PARAM (da Silva et al. 2006) was employed as they did, which determines the best stellar parameters and their errors by comparing the position on the HR diagram with grids of evolutionary tracks based on the Bayesian estimation method. We used the version 1.3 of PARAM, which returns *age*, M_{trk} , $\log g$, R , and $(B - V)_0$ along with their errors as output, for given 8 input parameters (observed values and errors of T_{eff} , $[\text{Fe}/\text{H}]$, $V_0 (\equiv V - A_V)$, and π). As to the errors of input parameters, while the actual error attached to each value was assigned for π , typical values of ± 100 K and ± 0.1 dex were uniformly assumed for T_{eff} and $[\text{Fe}/\text{H}]$, respectively (cf. Sect. 3.3 in T08). Regarding V_0 , since the main source of error is due to the uncertainty in A_V , ± 0.3 dex (103 *Kepler* giants; judged from the size of error bars in Fig. 2a) and ± 0.1 dex (11 nearby giants) were given.⁷

The resulting values of M_{trk} are presented in Table 1, while the complete input data and output results of PARAM⁸ are summarised in “PARAMresults.dat” of the online material. The M_{trk} values of 11 nearby stars derived in this study are compared with those of Ghezzi & Johnson (2015: cf. their Table 2) in Fig. 4. It can be seen from this figure that both determinations are almost consistent with each other, except for HD 185351 which shows some discrepancy due to the difference in $[\text{Fe}/\text{H}]$ (i.e., they used $+0.16$ in contrast to the adopted 0.00 derived in T08).

5 Discussion

5.1 M_{gLT} versus M_{trk}

We are now ready to discuss the quantitative reliability of M_{gLT} (derived by the straightforward model-independent approach) as well as of M_{trk} (determined

⁷The error of A_V (EXTINCT) is evaluated as the standard deviation of the mean of those derived by different subroutines (taken from various literature using different dust maps), as described in the header of the EXTINCT program. Such obtained error in A_V (EXTINCT) was further assumed to be equal to that of A_V (KIC), because there is no other way for estimating A_V (KIC) errors. Assigning ± 0.1 mag to V errors of nearby giants is just tentative, owing to the lack of information on errors in absolute photometry for such bright stars, though this may be a somewhat overestimation.

⁸In implementing PARAM1.3, the option of PARSEC version 1.1 (Bressan et al., 2012) was selected for the evolutionary tracks, and the default setting was applied unchanged for the Bayesian priors.

⁵Several recent studies have reported that small corrections should be applied to the original *Gaia* parallaxes. This effect is separately discussed in the Appendix.

⁶<http://asterisk.apod.com/library/ASCL/extinct/extinct.for>

with the help of theoretical evolutionary tracks) by comparing them with the reference M_{seis} values. In Fig. 5, these two kinds of stellar masses are plotted against M_{seis} , and the dependences of relative differences (logarithmic mass ratios) upon M_{seis} , $[\text{Fe}/\text{H}]$, and $\log L$ are also depicted, from which several characteristic trends of interest can be read.

Fig. 5a suggests that M_{gLT} correlates with M_{seis} , but the correlation is not so tight with a rather large dispersion (correlation coefficient is $+0.62$). Actually, the logarithmic mass ratio distributes at $-0.3 \lesssim \log(M_{gLT}/M_{\text{seis}}) \lesssim +0.3$ (as shown in Figs. 5b–5d) and its average is $\langle \log(M_{gLT}/M_{\text{seis}}) \rangle = +0.05$ (standard deviation is $\sigma = 0.14$). Accordingly, M_{gLT} by itself is not so sufficiently precise as to be practically usable with confidence. Meanwhile, since the disagreement of M_{gLT} relative to M_{seis} almost uniformly distribute without a significant dependence upon the stellar parameters (except that $\log(M_{gLT}/M_{\text{seis}})$ tends to increase with a decrease in mass at $M_{\text{seis}} \lesssim 1 M_{\odot}$; cf. Fig. 5b), it would be meaningful to discuss M_{gLT} values for a large number of stars altogether because errors may be statistically cancelled, which may be regarded as a point of merit.

On the other hand, M_{trk} shows opposite characteristics in the sense that whether it is consistent with M_{seis} apparently depends upon the evolutionary stage as manifestly seen in Figs. 5e–5h. That is, while a satisfactory agreement is observed in stars of RG (H-burning) and RC2 (He-burning, mass higher than $1.8 M_{\odot}$), M_{trk} is systematically larger than M_{seis} for the case of RC1 (He burning, mass lower than $1.8 M_{\odot}$).⁹ As a matter of fact, $\log(M_{\text{trk,RC1}}/M_{\text{seis}})$ significantly deviates from zero extending up to $\sim +0.4$ ($\langle \log(M_{\text{trk,RC1}}/M_{\text{seis}}) \rangle = +0.16$ with $\sigma = 0.11$), while the agreement with M_{seis} is fairly good for both $M_{\text{trk,RG}}$ and $M_{\text{trk,RC2}}$ ($\langle \log(M_{\text{trk,RG}}/M_{\text{seis}}) \rangle = -0.01$ with $\sigma = 0.06$ and $\langle \log(M_{\text{trk,RC2}}/M_{\text{seis}}) \rangle = -0.01$ with $\sigma = 0.08$). More precisely, those RC1 stars showing conspicuous deviations are confined in the luminosity range of $1.7 \lesssim \log(L/L_{\odot}) \lesssim 2.0$ (cf. Fig. 5h), and their masses are comparatively low in the range of $0.8 \lesssim M_{\text{seis}}/M_{\odot} \lesssim 1.5$ (cf. Fig. 5f). The reason for this problem is presumably attributed to the fact that RC1 tracks of lower mass (e.g., $\sim 1 M_{\odot}$) and RG/RC2 tracks of higher mass (e.g., $\sim 2 M_{\odot}$) are intricate with each other at this luminosity range (cf. Fig. 3). The double peak in the mass probability function inevitably caused by the degeneracy of tracks

would eventually result in an erroneous M_{trk} (though it is not straightforward to explain why overestimation of RC1 mass is preferentially observed but underestimation of RG/RC2 mass is not). Accordingly, Ghezzi & Johnson’s (2015) argument supporting the validity of M_{trk} determined for red giants with the help of evolutionary tracks is not necessarily correct, because M_{trk} is apt to be considerably overestimated for lower-mass RC1 stars at $1.7 \lesssim \log(L/L_{\odot}) \lesssim 2.0$, even though sufficient precision is surely attained (as they say) for stars of RG and RC2 stages. The reason why Ghezzi & Johnson (2015) did not detect appreciably large overestimation of M_{trk} (in comparison with M_{seis}) may be due to the difference in the mass distribution of sample stars. That is, since their program stars include only a small number of stars in the lower-mass range around $\sim 1 M_{\odot}$ (where RC1 giants show large mass discrepancies as revealed in this study) as seen from their Fig. 2, this problem may not have been particularly noticeable.

Combining what has been described above, we can summarise as follows regarding the merit and demerit of M_{gLT} and M_{trk} and how to make the best use of them.

- The precision of M_{gLT} itself is unfortunately insufficient for practical use, because errors on the order of several tens percent or more (~ 0.2 dex) are common. It is not recommendable to put much trust in its value.
- In contrast, M_{trk} is comparatively more reliable because its involved errors can be apparently smaller (typically within $\lesssim 10$ – 20% for the case of RG/RC2) but its weakpoint is that a considerable overestimation (even by $\gtrsim 100\%$ in unfortunate cases) takes place for a specific group (RC1) of stars.
- Therefore, since the evolutionary status of red giants is generally unknown, the hybrid approach utilising both together would be advisable, where larger weight may be placed to M_{trk} while M_{gLT} plays the checking role. Actually, spectroscopically determined atmospheric parameters (T_{eff} , $\log g$, and $[\text{Fe}/\text{H}]$) can be most effectively exploited by calculating both M_{gLT} (derived from L , $\log g$, and T_{eff}) and M_{trk} (determinable from L , $[\text{Fe}/\text{H}]$, and T_{eff}).
- Practically, M_{trk} would be allowed to adopt at first, though it should not be blindly trusted. Especially, one should be cautious for stars in the luminosity range of $1.7 \lesssim \log(L/L_{\odot}) \lesssim 2.0$. In such cases, it would be a useful check to compare M_{trk} and M_{gLT} with each other in order to avoid making serious errors.
- Although M_{gLT} does not have a sufficient precision by itself, this rather large uncertainty applies similarly to any star irrespective of the stellar types or

⁹Accordingly, this consequence (considerable $M_{\text{trk}} > M_{\text{seis}}$ discrepancy is seen for lower-mass RC1 giants of $M < 1.8 M_{\odot}$) apparently contradicts the result of Malla et al. (2020) who argued based on a sample of 16 giants that large overestimation of spectroscopic masses occurs for higher mass giants of $M > 1.6 M_{\odot}$.

parameters. As such, studying the general trends of M_{gLT} based on a large sample of stars may yield almost correct results, because random errors would be cancelled in such a statistical discussion.

5.2 Age–metallicity relation revisited with M_{gLT}

As an example of applying M_{gLT} to discussing the trends of many stars, the mass-dependent parameters of 322 mid-G to early-K giants studied in T08 were reinvestigated by using M_{gLT} . Actually, there was a problem in the consequence of that paper. Although M_{trk} was determined in T08 for each star by using Lejeune & Schaerer’s (2001) grids of evolutionary tracks, the resulting stellar age (closely associated with the mass) yielded an age–metallicity relation for giants seriously discrepant from that of dwarfs (cf. Fig. 14 therein). T15 revisited this problem and concluded that M_{trk} results of many (even if not all) clump giants determined in T08 are likely to be significantly overestimated (see also Appendix B in T16), leading to an underestimation of corresponding ages. It is thus interesting to see how the results would change if M_{gLT} is used instead of $M_{\text{trk},\text{T08}}$.

The values of M_{gLT} were determined for each of the 322 giants by using T_{eff} , $\log g$, and $\log L$ given in Table 1 of T08. The comparison between such obtained M_{gLT} and $M_{\text{trk},\text{T08}}$ is shown in Fig. 6a. Besides, how T_{eff} , $\log g$, $[\text{Fe}/\text{H}]$, and $\log L$ are related with M_{gLT} is depicted in Figs. 6b, 6c, 6d, and 6e, respectively (which should be compared with Figs. 3d, 3e, 3f, and 3a in T08). Further, the age of each star was derived from M_{gLT} by applying the approximate relation $\log \text{age} \simeq 10.74 - 1.04(M/M_{\odot}) + 0.0999(M/M_{\odot})^2$ (where age is in yr; cf. Sect. 3.2 in T08), and the resulting $[\text{Fe}/\text{H}]$ vs. age relation is displayed (along with that of dwarfs) in Fig. 6f.

Fig. 6a reveals that an inequality relation $M_{gLT} < M_{\text{trk},\text{T08}}$ holds at $M_{gLT} \lesssim 3 M_{\odot}$, which indicates that $M_{\text{trk},\text{T08}}$ was systematically overestimated in this mass range. The age derived by using M_{gLT} (instead of $M_{\text{trk},\text{T08}}$) results in a revised $[\text{Fe}/\text{H}]$ vs. age relation of giants, which is more consistent and well overlaps with that of dwarfs (Fig. 6f). This reasonably confirms the argument done in T15 (cf. Fig. 13 therein) that the discrepancy between giants and dwarfs would be effectively mitigated by the revision of M .

5.3 On the error source of M_{gLT}

As described in Sect. 5.1, the error involved in M_{gLT} turned out unfortunately somewhat too large for

the purpose of practical application. On the assumption of random errors in the Gaussian distribution, $\sigma(\log M_{gLT})$ is written as the root-sum-square of $\sigma(\log g)$, $\sigma(\log L)$, and $\sigma(4 \log T_{\text{eff}})$ according to Eq.(1). In the present case of red giants in the *Kepler* field, $\sigma(\log g) \sim 0.1$ (cf. Table 3 in T15), $\sigma(\log L) \sim 0.1$ (mainly determined by errors in A_V on the order of ~ 0.3 mag; cf. Sect. 4), and $\sigma(4 \log T_{\text{eff}}) \sim 0.04$ (corresponding to ~ 100 K). These values yield $\sigma(\log M_{gLT}) \sim \sqrt{0.1^2 + 0.1^2 + 0.04^2} \sim 0.15$, which is reasonably consistent with the standard deviation (0.14 dex) observed for the distribution of $\log(M_{gLT}/M_{\text{seis}})$.

Among these error terms, while $\sigma(\log L)$ may be brought down to the level of ~ 0.05 dex (if A_V is insignificant) and the contribution of $\sigma(4 \log T_{\text{eff}})$ is already small, $\sigma(\log g)$ is most important (essentially controlling the accuracy of M_{gLT}) but its further reduction would not be easy. On the contrary, this error may become more serious, because spectroscopic $\log g$ determination tends to sensitively depend upon technical details. Actually, the accuracy of $\log g$ appears to differ from case to case as seen from the comparison of various literature values (see Sect. 3.3 in T08). Therefore, the precision of $\sigma(\log g) \simeq 0.1$ accomplished in this investigation may not necessarily be guaranteed in other circumstances.

As an example to illustrate this situation, the atmospheric parameters spectroscopically determined by Luck (2015) based on Fe I and Fe II lines in his extensive study of 1133 FGK-type giants are compared with those of T08 in Fig. 7. It can be seen from Fig. 7b that the comparison between $\log g(\text{Luck})$ and $\log g(\text{T08})$ shows an appreciable systematic difference with a rather large dispersion as $\langle \Delta \log g \rangle(\text{Luck}-\text{T08}) = -0.18$ ($\sigma = 0.19$),¹⁰ despite that reasonable consistency is observed in other spectroscopic parameters (Figs. 7a, 7c, and 7d). As such, using $\log g$ derived by Luck (2015) would result in systematic underestimation of M_{gLT} (on the average by ~ 0.2 dex or $\sim 60\%$ along with an appreciably larger random dispersion) compared to the case based on $\log g(\text{T08})$.

¹⁰Although the cause of this discrepancy is not clear, the difference in the adopted set of Fe I and Fe II lines might be involved. The number of lines used by Luck (2015) amounts up to ~ 500 – 600 (Fe I) and ~ 50 – 60 (Fe II). These numbers are considerably larger (by a factor of ~ 2 – 3) compared to the case of the author’s previous studies (T08, T09, T15, T16, T19), where the adopted lines were limited to those weaker than $120 \text{ m}\text{\AA}$, because stronger ones affected by the effect of damping wings were intentionally avoided (as they tend to be problematic in view of the difficulty in equivalent-width measurements or uncertainties in damping parameters). Accordingly, if such stronger lines were included in Luck’s (2015) analysis, this might be the reason for the disagreement.

Accordingly, attention should be paid to the precision of $\log g$ in case of deriving M_{gLT} , for which confirming its quantitative reliability is prerequisite. It may be useful to carry out a test in advance on a number of benchmark giant stars with known seismic parameters (e.g., by using the spectra of *Kepler* giants published by Thygesen et al., 2012), in order to check the consistency between spectroscopic and seismic gravities.

6 Summary and conclusion

The conventional method for determining the mass of a star is to compare its location on the $\log L$ vs. T_{eff} diagram with grids of theoretical evolutionary tracks computed for various combinations of $(M, [\text{Fe}/\text{H}])$. This is occasionally called “spectroscopic mass determination” because T_{eff} and $[\text{Fe}/\text{H}]$ are to be established in advance (in addition to L determinable from the observed magnitude and the parallax) by the spectroscopic approach using Fe I and Fe II lines.

Recently, the validity of such track-based mass (M_{trk}) determined for red giant stars has been a controversial issue. That is, M_{trk} appears to be erroneously overestimated, which has been made known in comparison with the seismologically established mass (M_{seis}) of higher precision. However, practical details of this problem (e.g., how much error is expected in which type of giants) are still unclear.

In the meantime, another spectroscopic method for M determination is conceptually possible, which makes direct use of the surface gravity ($\log g$) along with L and T_{eff} to derive the mass (M_{gLT}). Although this approach is simple and straightforward, it has barely been applied so far in practice, presumably because of the lack of reliability on $\log g$.

However, the author has come to develop some confidence on the surface gravity values of red giants determined from Fe I and Fe II lines in his previous studies, because spectroscopic $\log g$ determined for giants in the *Kepler* field turned out to be consistent with seismic $\log g$ (T15, T16).

It was therefore decided to evaluate M_{gLT} for those ~ 100 *Kepler* giants (sample stars in T15 and T16), for which M_{seis} as well as the evolutionary status (RG or RC1 or RC2) are already known, in order to examine the accuracy of M_{gLT} . In addition, M_{trk} values were also determined for all the program stars by using the PARAM code (da Silva et al. 2006) for the purpose of clarifying the reliability of M_{trk} under dispute. The necessary parameters (T_{eff} , $\log g$, $[\text{Fe}/\text{H}]$) were taken from the previous work (mainly T15 and T16) and L values were derived by using the parallaxes (mainly from *Gaia* DR2).

We could confirm a positive correlation between M_{gLT} and M_{seis} (with a correlation coefficient of +0.62), but $\log(M_{gLT}/M_{\text{seis}})$ distribute over a wide range between ~ -0.3 and $\sim +0.3$ (it average is +0.05 with $\sigma = 0.14$). Therefore, the precision of M_{gLT} by itself is rather insufficient for practical use, because errors on the order of several tens percent or more (~ 0.2 dex) are quite common. However, since this rather large uncertainty applies similarly to any star irrespective of its type, studying the general trends of M_{gLT} based on a large sample of stars may still be meaningful because random errors would be cancelled.

On the other hand, the trend of M_{trk} was found to be in marked contrast to the case of M_{gLT} , in the sense that it critically depends on the type of stars. Regarding RG and RC2 stars, the precision of M_{trk} is quite satisfactory because its error is typically within $\lesssim 10$ –20% as seen from the distribution of $\log(M_{\text{trk}}/M_{\text{seis}})$ (the mean is -0.01 and the standard deviation is 0.06 – 0.08). However, for the case of RC1 stars (with comparatively lower mass of $0.8 \lesssim M_{\text{seis}}/M_{\odot} \lesssim 1.5$) at the luminosity range of $1.7 \lesssim \log(L/L_{\odot}) \lesssim 2.0$, M_{trk} is considerably higher than M_{seis} with the difference amounting up to $\sim 100\%$ or more, which means that M_{trk} is erroneously overestimated in this type of stars.

Accordingly, since the evolutionary status of red giants is generally unknown in advance, the hybrid approach utilising both M_{gLT} and M_{trk} in combination may be useful. M_{trk} may be preferably adopted in the first place, though utmost care should be taken for stars of $\log(L/L_{\odot}) \sim 1.7$ – 2.0 , while M_{gLT} may be secondarily employed to check if M_{trk} is not erroneously overestimated.

As an application of the potential merit of M_{gLT} mentioned above, the age–metallicity relation of 322 red giants studied in T08 was revisited by using M_{gLT} (instead of $M_{\text{trk},\text{T08}}$ which was later found to be rather overestimated) as the mass of each star. The new *age* vs. $[\text{Fe}/\text{H}]$ relation for 322 giants based on the revised mass values turned out to considerably mitigate the serious mismatch between giants and dwarfs reported in T08, indicating that statistically meaningful results may be obtained by using M_{gLT} .

The precision of M_{gLT} is essentially determined by the accuracy of $\log g$. However, since spectroscopic $\log g$ determination based on Fe I and Fe II lines is a delicate procedure sensitively dependent upon the technical details (e.g., selection of adopted lines), accomplishing a sufficient precision is not necessarily easy. Therefore, in case of deriving M_{gLT} by using Eq.(1), quantitative reliability of $\log g$ has to be confirmed in the first place.

Acknowledgments

This research has been carried out by using the SIMBAD database, operated by CDS, Strasbourg, France. For the purpose of mass determination in comparison with evolutionary tracks, the open software PARAM (ver.1.3) was used via the web interface at the PARAM site maintained by Dr. Leo Girardi.

References

- Alonso, A., Arribas, S., & Martínez-Roger, C. 1999, *Astron. Astrophys. Suppl. Ser.*, 140, 261
- Bailer-Jones, C. A. L., Rybizki, J., Fouesneau, M., Man-telet, G., & Andrae, R. 2018, *Astron. J.*, 156, 58
- Bressan, A., Marigo, P., Girardi, L., Salasnich, B., Dal Cero, C., Rubele, S., & Nanni, A. 2012, *Mon. Not. R. Astron. Soc.*, 427, 127
- Bressan, A., Marigo, P., Girardi, L., Nanni, A., & Rubele, S. 2013, *EPJ Web of Conferences*, 43, 3001 (DOI: <http://dx.doi.org/10.1051/epjconf/20134303001>)
- Brewer, J. M., Fischer, D. A., Basu, S., Valenti, J. A., & Piskunov, N. 2015, *Astrophys. J.*, 805, 126
- Brown, T. M., Latham, D. W., Everett, M. E., & Esquerdo, G. A. 2011, *Astron. J.*, 142, 112
- da Silva, L., et al. 2006, *Astron. Astrophys.*, 458, 609
- Gaia Collaboration, et al. 2016, *Astron. Astrophys.*, 595, A1
- Gaia Collaboration, et al. 2018, *Astron. Astrophys.*, 616, A1
- Campante, T. L., et al. 2017, *Mon. Not. R. Astron. Soc.*, 469, 1360
- Ghezzi, L., & Johnson, J. A. 2015, *Astrophys. J.*, 812, 96
- Ghezzi, L., Montet, B. T., & Johnson, J. A. 2018, *Astrophys. J.*, 860, 109
- Girardi, L., Bressan, A., Bertelli, G., & Chiosi, C. 2000, *Astron. Astrophys. Suppl. Ser.*, 141, 371
- Hakkila, J., Myers, J. M., Stidham, B. J., & Hartmann, D. H. 1997, *Astron. J.*, 114, 2043
- Hjørringgaard, J. G., Silva Aguirre, V., White, T. R., Huber, D., Pope, B. J. S., Casagrande, L., Justesen, A. B., & Christensen-Dalsgaard, J. 2017, *Mon. Not. R. Astron. Soc.*, 464, 3713
- Johnson, J. A., et al. 2007, *Astrophys. J.*, 665, 785
- Johnson, J. A., et al. 2014, *Astrophys. J.*, 794, 15
- Lejeune, T., & Schaerer, D. 2001, *Astron. Astrophys.*, 366, 538
- Lloyd, J. P. 2011, *Astrophys. J.*, 739, L49
- Lloyd, J. P. 2013, *Astrophys. J.*, 774, L2
- Luck, R. E. 2015, *Astron. J.*, 150, 88
- Malla, S. P., et al. 2020, *Mon. Not. R. Astron. Soc.*, 496, 5423
- Mosser, B., et al. 2012, *Astron. Astrophys.*, 540, A143
- North, T. S. H., et al. 2017, *Mon. Not. R. Astron. Soc.*, 472, 1866
- Schlaufman, K. C., & Winn, J. N. 2013, *Astrophys. J.*, 772, 143
- Sousa, S. G., et al. 2015, *Astron. Astrophys.*, 576, A94
- Stello, D., et al. 2017, *Mon. Not. R. Astron. Soc.*, 472, 4110
- Takeda, Y. 2007, *Publ. Astron. Soc. Jpn.*, 59, 335
- Takeda, Y., Hashimoto, O., & Honda, S. 2018, *Astrophys. J.*, 862, 57 (T18)
- Takeda, Y., Kaneko, H., Matsumoto, N., Oshino, S., Ito, H., & Shibuya, T. 2009, *Publ. Astron. Soc. Jpn.*, 61, 563 (T09)
- Takeda, Y., Ohkubo, M., & Sadakane, K. 2002, *Publ. Astron. Soc. Jpn.*, 54, 451
- Takeda, Y., Ohkubo, M., Sato, B., Kambe, E., & Sadakane, K. 2005, *Publ. Astron. Soc. Jpn.*, 57, 27 (Erratum 57, 415)
- Takeda, Y., Sato, B., & Murata, D. 2008, *Publ. Astron. Soc. Jpn.*, 60, 781 (T08)
- Takeda, Y., & Tajitsu, A. 2015, *Mon. Not. R. Astron. Soc.*, 450, 397 (T15)
- Takeda, Y., Tajitsu, A., Sato, B., Liu, Y.-J., Chen, Y.-Q., & Zhao, G. 2016, *Mon. Not. R. Astron. Soc.*, 457, 4454 (T16)
- Thygesen, A. O., et al. 2012, *Astron. Astrophys.*, 543, A160
- Torres, G., Claret, A., Pavlovski, K., & Dotter, A. 2015, *Astrophys. J.*, 807, 26
- Valenti, J. A., & Fischer, D. A. 2005, *Astrophys. J. Suppl. Ser.*, 159, 141
- White, T. R., et al. 2018, *Mon. Not. R. Astron. Soc.*, 477, 4403
- Wolthoff, V., Reffert, S., Quirrenbach, A., Jones, M. I., Wittenmyer, R. A., & Jenkins, J. S. 2022, *Astron. Astrophys.*, in press (arXiv: 2202.12800)
- Zinn, J. C., Pinsonneault, M. H., Huber, D., & Stello, D. 2019, *Astrophys. J.*, 878, 136

Data availability

Regarding the open software tools (TGVIT, EX-TINCT, PARAM), which are closely related to the contents of this article, their URLs are given in the footnotes of the main text. The fundamental data (equivalent widths, abundances, atomic data) of Fe I and Fe II lines, based on which the atmospheric parameters used in this study were spectroscopically determined, are given in the electronic tables of the previous papers of the author (referenced in Table 1).

Supplementary information

The following online data (electronic data tables) are available as supplementary materials of this article, which gives the fundamental data and the final results of this investigation.

- [readme.txt](#)
- [stellar_parameters.dat](#)
- [PARAMresults.dat](#)

Statements and declarations

Funding

The author declares that no funds, grants, or other support were received during the preparation of this manuscript.

Competing interests

The author has no relevant financial or non-financial interests to disclose.

Author contributions

This investigation has been conducted solely by the author.

Appendix: Effect of parallax correction on mass determination

Regarding the parallax data necessary for evaluating L (luminosity) by using Eq.(3), we invoked *Gaia* DR2 values (π_{Gaia}) for all of the 103 giants in the *Kepler* field. After the release of these *Gaia* data, several studies argued the possibility of small zero-point offset to be applied to π_{Gaia} . It is interesting to examine the impact of such small π corrections in mass determination, given that evaluation of M_{trk} from intricate evolutionary tracks may be sensitive to a slight change in L .

Zinn et al. (2019) reported based on asteroseismic data of red giants in the *Kepler* field that zero-point offset exists in the *Gaia* DR2 parallaxes, which depends on *Gaia* astrometric pseudocolour (ν_{eff}) and *Gaia* G -band magnitude. According to the formula derived by them, the values of this offset ($\pi_{\text{Zinn}} - \pi_{\text{Gaia}}$) for each of our 103 *Kepler* giants ($\nu_{\text{eff}} \sim 1.5\text{--}1.6$, $G \sim 6.7\text{--}12.1$; cf. Fig. 8a) turned out $\sim 0.05\text{--}0.06$ m.a.s. as shown in Fig. 8b. This amount of slight increase in π leads to a decrease in $\log L$ by $\lesssim 0.01\text{--}0.02$ dex ($-0.4 \log(\pi_{\text{Zinn}}/\pi_{\text{Gaia}})$). Although such a small change in $\log L$ has a negligible effect in M_{gLT} (only a few per cent at most), it might have an appreciable impact on M_{trk} . We thus conducted a test determination of M_{trk} again based on PARAM but adopting π_{Zinn} instead of π_{Gaia} (other input parameters were kept unchanged). The resulting mass values (M_{trk}^Z) are compared with those of original π_{Gaia} -based M_{trk} in Fig. 8c, where appreciable deviations (up to $\lesssim 20\text{--}30\%$) are observed for some cases despite a reasonable correlation overall. A closer inspection revealed that such problematic stars are seen in the luminosity range of $\log(L/L_{\odot}) \sim 1.5\text{--}2.0$ (cf. upper inset of Fig. 8d), which almost coincides with the region of large discrepancies between M_{trk} and M_{seis} (cf. Sect. 5.1). Accordingly, this effect of M_{trk} changes due to π correction is eventually inconspicuous in the $\log(M_{\text{trk}}/M_{\text{seis}})$ vs. $\log L$ diagram (Fig. 8d), because stars showing appreciable differences (up to $\log(M_{\text{trk}}^Z/M_{\text{trk}}) \lesssim 0.1$ dex) just fall in the luminosity region where the dispersion is already large, as can be

confirmed by comparing Fig. 8d with Fig. 5h (both appear almost similar). As such, we may state that the essential conclusion is not affected at all by using π_{Zinn} instead of π_{Gaia} .

Throughout this study, the distance (d) was derived as the reciprocal of the parallax ($1/\pi$) as usually done. However, Bailer-Jones et al. (2018) argued that distances obtained by simply inverting the *Gaia* DR2 parallaxes may suffer appreciable errors. Since this effect becomes progressively more significant with an increase in σ_{π}/π (see Fig. 6 in Bailer-Jones et al., 2018; σ_{π} is the error of π), it may be less significant in the present case where σ_{π}/π is only several per cent at most. Anyway, we also checked how much correction is expected for our *Kepler*-field giants, because the revised distance data (d_{Bailer}) are available in Bailer-Jones et al.’s (2018) catalogue. Fig. 8e shows that the difference between d_{Bailer} and d_{Gaia} ($\equiv 1/\pi_{\text{Gaia}}$; adopted in this study) is almost zero at small d but systematically grows towards larger d . Interestingly, in terms of the “pseudo”-parallax (formally derived as $\pi_{\text{Bailer}}^* \equiv d_{\text{Bailer}}^{-1}$), the difference between these two ($\pi_{\text{Bailer}}^* - \pi_{\text{Gaia}}$) is almost constant at $\simeq +0.03$ m.a.s. (Fig. 8f), which means that this effect is equivalent to the zero-point offset of π as long as our program stars are concerned. Considering that this offset is half as small as that of Zinn et al. (2019) discussed above, we may similarly state that it does not have any significant impact on our final conclusion.

Table 1 Basic data and the resulting parameters of 114 program stars.

Obj. name (1)	T_{eff} (2)	$\log g$ (3)	[Fe/H] (4)	Ref. (5)	V (6)	A_V (7)	π (8)	BC (9)	$\log L$ (10)	M_{gLT} (11)	M_{seis} (12)	M_{trk} (13)	Class (14)
KIC 01726211	4983	2.49	-0.57	T15	11.16	0.44	0.746	-0.27	1.973	1.91	1.19	1.61	RC1
KIC 02013502	4913	2.69	-0.02	T15	11.52	0.58	0.680	-0.29	1.977	3.23	1.94	2.59	RC2
KIC 02303367	4600	2.39	+0.06	T15	10.41	0.30	1.304	-0.43	1.798	1.40	1.23	1.49	RC1
KIC 02424934	4792	2.48	-0.18	T15	10.55	0.46	1.004	-0.34	1.996	2.30	1.36	2.20	RC1
KIC 02448225	4577	2.37	+0.16	T15	11.07	0.39	0.906	-0.44	1.892	1.69	1.87	1.97	RC2
KIC 02573092	4688	2.48	+0.00	T16	11.70	0.56	0.692	-0.39	1.920	2.11	1.43	2.04	RC1
KIC 02696732	4820	2.90	-0.13	T16	12.64	0.45	1.038	-0.33	1.122	0.79	1.33	1.15	RG
KIC 02714397	4910	2.56	-0.47	T15	10.75	0.43	1.020	-0.29	1.873	1.89	1.12	1.35	RC1
KIC 02988638	4912	2.67	+0.06	T16	12.15	0.50	0.597	-0.29	1.804	2.07	2.31	2.17	RC2
KIC 03098045	4820	2.34	-0.24	T16	12.18	0.49	0.552	-0.33	1.872	1.22	1.11	1.53	RC1
KIC 03217051	4590	2.44	+0.21	T15	11.87	0.41	0.714	-0.44	1.783	1.53	1.22	1.59	RC1
KIC 03323943	4826	2.55	-0.14	T16	11.95	0.51	0.648	-0.32	1.829	1.79	1.01	1.57	RC1
KIC 03425476	4780	2.57	-0.03	T16	12.56	0.39	0.604	-0.34	1.606	1.16	1.37	1.55	RC1
KIC 03455760	4654	2.68	-0.07	T15	11.39	0.43	1.024	-0.40	1.654	1.86	1.63	1.18	RG
KIC 03531478	5000	3.20	-0.06	T16	12.00	0.29	1.384	-0.26	1.040	1.13	1.50	1.28	RG
KIC 03730953	4861	2.55	-0.07	T15	9.06	0.19	1.869	-0.31	1.934	2.21	1.97	2.44	RC2
KIC 03744043	4946	2.94	-0.35	T15	9.81	0.34	2.476	-0.28	1.437	1.61	1.31	1.26	RG
KIC 03748691	4762	2.53	+0.11	T15	12.25	0.66	0.601	-0.35	1.847	1.88	1.37	2.25	RC1
KIC 03758458	5009	2.71	+0.07	T15	11.39	0.55	0.658	-0.26	2.029	3.53	2.18	2.75	RC2
KIC 04036007	4916	2.42	-0.36	T15	11.72	0.43	0.607	-0.29	1.933	1.56	1.38	1.74	RC1
KIC 04039306	4806	2.45	-0.10	T16	11.68	0.51	0.647	-0.33	1.944	1.88	1.03	2.28	RC1
KIC 04044238	4519	2.38	+0.20	T15	7.80	0.14	4.131	-0.48	1.796	1.46	1.06	1.57	RC1
KIC 04056266	5021	2.67	-0.03	T16	12.67	0.49	0.617	-0.25	1.548	1.05	2.25	1.96	RC2
KIC 04243623	5005	3.75	-0.31	T15	11.40	0.14	2.830	-0.26	0.599	1.44	0.99	1.00	RG
KIC 04243796	4620	2.34	+0.11	T15	10.86	0.38	1.000	-0.42	1.877	1.46	1.26	1.95	RC1
KIC 04350501	4929	3.19	-0.09	T16	11.89	0.50	1.126	-0.28	1.355	2.41	1.63	1.40	RG
KIC 04351319	4876	3.32	+0.29	T15	10.19	0.15	3.812	-0.30	0.842	1.04	1.45	1.27	RG
KIC 04445711	4876	2.50	-0.32	T15	11.06	0.36	0.938	-0.31	1.799	1.43	1.35	1.35	RC1
KIC 04448777	4805	3.19	+0.10	T16	11.87	0.33	1.579	-0.33	1.018	1.23	1.13	1.21	RG
KIC 04570120	5035	2.73	+0.05	T16	11.46	0.48	0.613	-0.25	2.032	3.65	2.44	2.75	RC2
KIC 04726049	5028	3.25	-0.16	T16	12.14	0.48	1.329	-0.25	1.091	1.39	1.37	1.26	RG
KIC 04770846	4847	2.60	+0.02	T15	9.77	0.33	1.604	-0.32	1.840	2.02	1.58	2.28	RC1
KIC 04902641	4986	2.84	+0.03	T15	11.14	0.29	1.085	-0.26	1.594	1.78	2.56	2.00	RC2
KIC 04952717	4793	3.13	+0.13	T15	11.69	0.42	1.905	-0.34	0.966	0.96	1.24	1.20	RG
KIC 05000307	5023	2.64	-0.25	T15	11.43	0.46	0.706	-0.25	1.915	2.28	1.41	2.27	RC1
KIC 05033245	5049	3.41	+0.11	T15	11.24	0.19	2.389	-0.24	0.823	1.07	1.41	1.33	RG
KIC 05088362	4760	2.41	+0.03	T15	11.38	0.41	0.622	-0.35	2.064	2.35	2.22	2.67	RC2
KIC 05128171	4808	2.54	+0.04	T15	10.37	0.42	1.248	-0.33	1.862	1.91	2.03	2.32	RC2
KIC 05266416	4767	2.50	-0.09	T15	10.80	0.39	1.001	-0.35	1.875	1.86	1.51	1.86	RC1
KIC 05283798	4770	2.53	+0.09	T16	12.13	0.50	0.593	-0.35	1.842	1.84	1.79	2.14	RC2
KIC 05307747	5030	2.77	+0.01	T15	8.67	0.21	2.731	-0.25	1.745	2.07	2.91	2.11	RC2
KIC 05514974	4674	2.26	-0.10	T16	11.57	0.43	0.785	-0.39	1.809	0.99	1.03	1.42	RC1
KIC 05530598	4599	2.85	+0.37	T15	8.93	0.23	3.986	-0.43	1.393	1.59	1.68	1.34	RG
KIC 05598645	5052	3.44	-0.17	T16	12.10	0.34	1.406	-0.25	1.000	1.71	1.14	1.23	RG
KIC 05611192	5064	2.91	+0.02	T16	12.12	0.49	0.611	-0.24	1.771	2.95	2.43	2.22	RC2
KIC 05723165	5255	3.67	-0.02	T15	10.87	0.26	3.130	-0.19	0.742	1.37	1.36	1.35	RG
KIC 05737655	5026	2.45	-0.63	T15	7.31	0.17	4.964	-0.26	1.756	1.02	0.78	1.00	RC1
KIC 05795626	4923	2.38	-0.72	T15	9.39	0.25	1.530	-0.29	1.993	1.63	1.21	1.40	RC1
KIC 05806522	4574	2.60	+0.12	T15	11.33	0.40	1.038	-0.45	1.675	1.74	1.18	1.25	RG
KIC 05858034	4887	2.45	-0.19	T16	12.06	0.44	0.558	-0.30	1.880	1.52	1.27	1.89	RC1
KIC 05866737	4874	2.86	-0.26	T15	10.91	0.42	1.198	-0.31	1.670	2.43	1.52	1.35	RG
KIC 05990753	5010	2.97	+0.19	T15	11.04	0.58	1.010	-0.26	1.810	3.88	2.70	2.42	RC2
KIC 06117517	4649	2.94	+0.28	T15	10.78	0.40	1.887	-0.41	1.356	1.72	1.26	1.31	RG
KIC 06144777	4734	3.02	+0.14	T15	11.22	0.31	1.955	-0.37	1.100	1.06	1.18	1.22	RG
KIC 06276948	4939	2.84	+0.19	T15	11.28	0.34	0.959	-0.28	1.672	2.21	2.35	2.06	RC2
KIC 06531928	5156	3.73	-0.57	T16	10.97	0.19	3.211	-0.22	0.662	1.41	0.95	0.95	RG
KIC 06579495	4772	2.78	-0.02	T16	12.20	0.36	0.902	-0.35	1.392	1.16	1.22	1.30	RG
KIC 06665058	4750	3.10	-0.07	T16	11.47	0.38	1.282	-0.36	1.390	2.46	1.18	1.24	RG
KIC 06690139	4979	3.02	-0.14	T15	11.86	0.35	0.898	-0.27	1.498	2.17	1.56	1.71	RG
KIC 07205067	5064	2.58	+0.03	T15	10.80	0.32	0.725	-0.24	2.085	2.85	3.49	2.82	RC2
KIC 07341231	5305	3.65	-1.73	T16	10.05	0.14	4.225	-0.22	0.772	1.35	0.73	0.80	RG

Table 1 (Continued.)

Obj. name (1)	T_{eff} (2)	$\log g$ (3)	[Fe/H] (4)	Ref. (5)	V (6)	A_V (7)	π (8)	BC (9)	$\log L$ (10)	M_{gLT} (11)	M_{seis} (12)	M_{trk} (13)	Class (14)
KIC 07581399	5070	2.74	+0.01	T15	11.54	0.36	0.586	-0.24	1.988	3.28	3.13	2.65	RC2
KIC 07584122	4974	3.29	-0.08	T16	11.65	0.29	1.223	-0.27	1.290	2.52	1.26	1.41	RG
KIC 07734065	4882	2.20	-0.43	T16	12.04	0.43	0.499	-0.31	1.982	1.09	0.93	1.65	RC1
KIC 07799349	4969	3.56	+0.28	T16	9.67	0.12	5.434	-0.27	0.717	1.26	1.31	1.29	RG
KIC 08378462	4995	2.81	+0.06	T15	11.40	0.53	0.878	-0.26	1.769	2.47	2.47	2.22	RC2
KIC 08475025	4848	2.88	-0.06	T16	12.06	0.34	0.939	-0.32	1.394	1.38	1.41	1.36	RG
KIC 08493735	5842	3.62	+0.01	T16	10.25	0.17	3.187	-0.08	0.893	1.13	1.05	1.47	RG
KIC 08702606	5472	3.66	-0.11	T15	9.51	0.04	5.496	-0.14	0.688	1.01	1.09	1.26	RG
KIC 08718745	4902	3.20	-0.25	T15	11.10	0.30	1.994	-0.30	1.100	1.40	1.17	1.13	RG
KIC 08751420	5260	3.63	-0.15	T16	7.01	0.05	17.176	-0.19	0.722	1.19	1.08	1.27	RG
KIC 08813946	4862	2.64	+0.09	T15	7.19	0.14	5.309	-0.31	1.753	1.79	2.09	2.02	RC1
KIC 09145955	4943	2.85	-0.34	T16	10.05	0.28	2.384	-0.28	1.350	1.08	1.39	1.21	RG
KIC 09173371	5064	2.85	+0.00	T15	9.59	0.37	2.111	-0.24	1.657	1.98	2.32	2.04	RC2
KIC 09349632	4976	2.75	+0.12	T16	11.37	0.38	0.600	-0.27	2.052	4.19	2.60	2.81	RC2
KIC 09583430	4854	2.73	+0.21	T16	12.03	0.46	0.733	-0.31	1.666	1.82	2.62	1.95	RC2
KIC 09705687	5129	2.81	-0.19	T15	9.80	0.28	1.494	-0.22	1.835	2.58	1.92	2.21	RC2
KIC 09812421	5140	3.48	-0.21	T16	10.32	0.18	3.327	-0.22	0.887	1.35	1.27	1.23	RG
KIC 10323222	4525	2.43	+0.04	T15	7.02	0.08	7.366	-0.48	1.578	0.99	1.55	1.25	RG
KIC 10382615	4890	2.25	-0.49	T16	12.02	0.36	0.528	-0.30	1.911	1.03	1.00	1.40	RC1
KIC 10404994	4802	2.63	-0.06	T15	7.66	0.12	4.103	-0.33	1.791	2.01	1.50	1.65	RC1
KIC 10426854	4968	2.52	-0.30	T15	10.31	0.32	1.399	-0.27	1.724	1.17	1.78	1.35	RC1
KIC 10474071	4975	2.65	+0.09	T16	12.02	0.50	0.627	-0.27	1.805	1.89	2.38	2.34	RC2
KIC 10600926	4879	2.48	-0.20	T16	11.88	0.47	0.627	-0.30	1.865	1.58	0.82	1.74	RC1
KIC 10604460	4573	2.37	+0.14	T16	11.02	0.41	0.881	-0.45	1.945	1.91	1.26	2.08	RC1
KIC 10709799	4522	2.51	-0.04	T16	11.29	0.30	1.086	-0.48	1.623	1.32	1.29	1.21	RG
KIC 10716853	4874	2.55	-0.08	T15	7.04	0.10	5.386	-0.31	1.783	1.54	1.75	1.74	RC1
KIC 10866415	4791	2.82	-0.01	T16	11.52	0.44	1.378	-0.34	1.325	1.08	1.25	1.29	RG
KIC 11177749	4677	2.24	-0.04	T16	11.23	0.33	0.894	-0.39	1.794	0.92	1.20	1.44	RC1
KIC 11251115	4837	2.57	+0.07	T16	8.09	0.16	3.088	-0.32	1.877	2.07	2.45	2.43	RC2
KIC 11352756	4604	2.29	-0.04	T16	11.22	0.47	0.878	-0.43	1.883	1.34	0.86	1.57	RC1
KIC 11401156	5053	3.58	+0.10	T16	10.01	0.13	4.807	-0.24	0.682	1.14	1.09	1.27	RG
KIC 11444313	4757	2.52	+0.00	T15	11.65	0.40	0.678	-0.35	1.880	1.99	1.39	2.12	RC1
KIC 11569659	4879	2.48	-0.26	T15	11.57	0.58	0.647	-0.31	2.003	2.18	0.85	2.28	RC1
KIC 11618103	4922	2.91	-0.17	T16	7.93	0.16	6.176	-0.29	1.326	1.19	1.41	1.30	RG
KIC 11657684	4951	2.47	-0.12	T15	12.00	0.46	0.548	-0.28	1.914	1.63	1.27	2.39	RC1
KIC 11717120	5087	3.72	-0.31	T16	9.49	0.12	6.932	-0.24	0.565	1.17	1.14	1.00	RG
KIC 11721438	4959	2.87	+0.14	T16	12.04	0.48	0.674	-0.27	1.729	2.66	2.40	2.14	RC2
KIC 11802968	4962	3.73	-0.06	T16	11.22	0.23	3.327	-0.27	0.569	1.33	0.81	1.09	RG
KIC 11819760	4824	2.36	-0.18	T15	11.27	0.36	0.692	-0.33	1.986	1.66	1.25	2.27	RC1
KIC 12008680	4881	2.55	-0.32	T16	11.49	0.45	0.732	-0.30	1.877	1.91	0.81	1.56	RC1
KIC 12070114	4698	2.46	+0.05	T16	11.05	0.35	0.817	-0.38	1.949	2.13	1.78	2.31	RC2
KIC 12884274	4683	2.44	+0.11	T15	7.88	0.20	3.713	-0.39	1.844	1.62	1.39	2.10	RC1
HD 107383	4841	2.51	-0.28	T08	4.74	0.02	10.710	-0.32	2.081	2.88	2.48	2.21	—
HD 124897	4281	1.72	-0.55	T09	-0.05	0.00	88.830	-0.64	2.280	1.21	0.69	1.04	—
HD 062509	4904	2.84	+0.06	T08	1.14	0.00	96.540	-0.29	1.592	1.90	2.31	2.00	—
HD 146791	4931	2.69	-0.07	T08	3.23	0.00	30.640	-0.28	1.749	1.88	1.93	1.75	—
HD 168723	4972	3.12	-0.18	T08	3.25	0.00	53.930	-0.27	1.245	1.54	1.82	1.29	—
HD 219615	4802	2.25	-0.62	T08	3.70	0.04	23.640	-0.34	1.822	0.90	1.03	1.12	—
HD 185351	5006	3.16	+0.00	T08	5.17	0.05	24.225	-0.26	1.187	1.43	2.03	1.43	—
HD 028307	4924	2.63	+0.10	T08	3.84	0.00	21.130	-0.29	1.829	1.98	2.96	2.39	—
HD 076294	4844	2.30	-0.11	T08	3.10	0.00	19.510	-0.32	2.206	2.36	3.15	2.91	—
Capella(P)	4943	2.52	+0.10	T18	0.92	0.00	76.200	-0.28	1.880	1.70	2.57	2.50	—
Capella(S)	5694	2.88	-0.08	T18	0.75	0.00	76.200	-0.10	1.878	2.21	2.49	2.47	—

(1) Object name. (2) Effective temperature (in K). (3) Logarithmic surface gravity (c.g.s. unit, in dex). (4) Logarithmic Fe abundance relative to the Sun (in dex). (5) References for the spectroscopically determined parameters given in (2)–(4): T08 ... Takeda, Sato & Murata (2008), T09 ... Takeda et al. (2009), T15 ... Takeda & Tajitsu (2015), T16 ... Takeda et al. (2016), and T18 ... Takeda, Hashimoto & Honda (2018). (6) Apparent visual magnitude (in mag), where those of Capella's primary and secondary components were derived by adopting the flux ratio of $f_P/f_S = 0.85$ at 5500 Å (cf. Fig. 1 in Torres et al., 2015). (7) Interstellar extinction (in mag). (8) Trigonometric parallax (in milliarcsecond). (9) Bolometric correction (in mag). (10) Logarithmic bolometric luminosity (in unit of L_\odot). (11) Stellar mass derived from g , L , and T_{eff} by using Eq.(1). (12) Reference mass values determined by the seismic technique (except for those of the binary system Capella, which were derived from their orbital motions). (13) Stellar mass derived from the positions on the HR diagram in comparison with theoretical evolutionary tracks by using PARAM. (14) Evolutionary class of each *Kepler* giant seismologically determined by Mosser et al. (2012) (RG: red giant, RC1: 1st clump giant, RC2: 2nd clump giant).

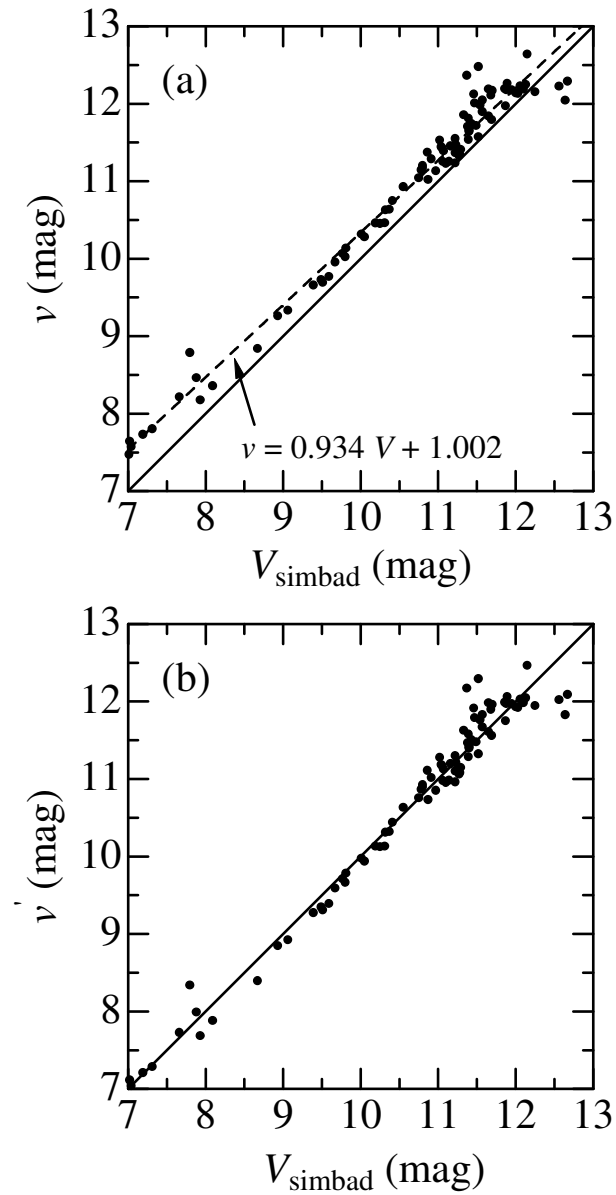


Fig. 1 (a) The visual-band magnitudes (v), which were tentatively estimated for the *Kepler* giants based on the r -band magnitudes given in *Kepler* Input Catalogue (Brown et al., 2011) by using the theoretical $V - R$ indices of Giraldi et al.'s (2000) stellar evolution calculations, plotted against the actual V magnitudes taken from the SIMBAD database. The linear-regression relation ($v = 0.934V + 1.002$) is also depicted by the dashed line. (b) The corrected v' values are plotted against V , where $v' \equiv (v - 1.002)/0.934$.

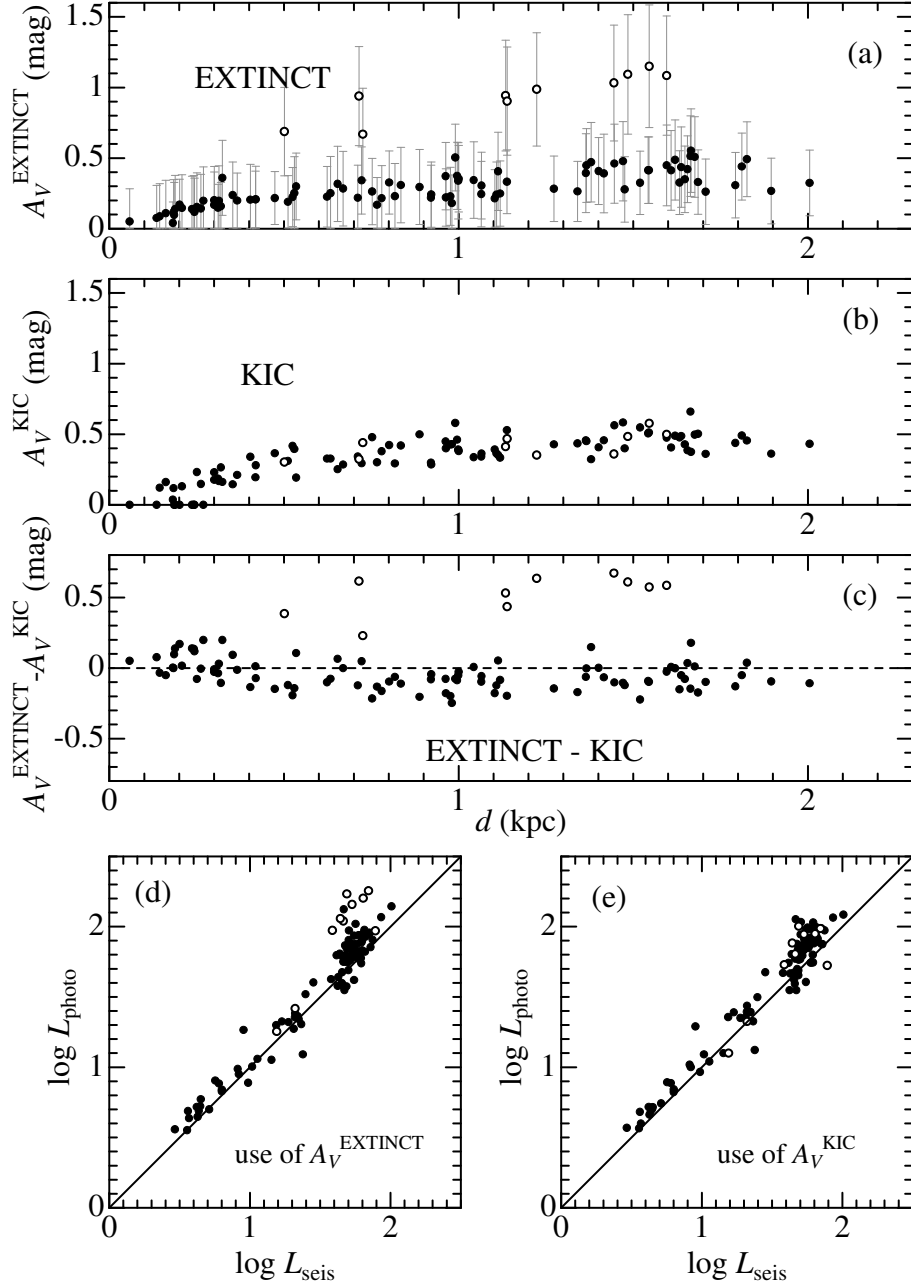


Fig. 2 (a) Visual extinction values (A_V^{EXTINCT}), which were evaluated with the help of the EXTINCT code (Hakkila et al., 1997) for the 103 *Kepler* giants, plotted against the distance, where error bars indicate the total extinction errors given by EXTINCT. (b) A_V^{KIC} values of *Kepler* giants, which are given in the *Kepler* Input Catalogue (Brown et al., 2011), plotted against the distance. (c) Difference between A_V^{EXTINCT} and A_V^{KIC} , plotted against the distance. (d) Luminosities of *Kepler* giants (L_{photo}) photometrically derived based on Eq.(2) with A_V^{EXTINCT} are compared with those (L_{seis}) derived in T15 and T16 by using R_{seis} (seismic radius). (e) L_{photo} values of *Kepler* giants obtained by using A_V^{KIC} are plotted against L_{seis} . In each panel, 10 stars showing appreciable deviations of A_V^{EXTINCT} from the main trend in panel (a) are plotted by open symbols, in order to distinguish them from others.

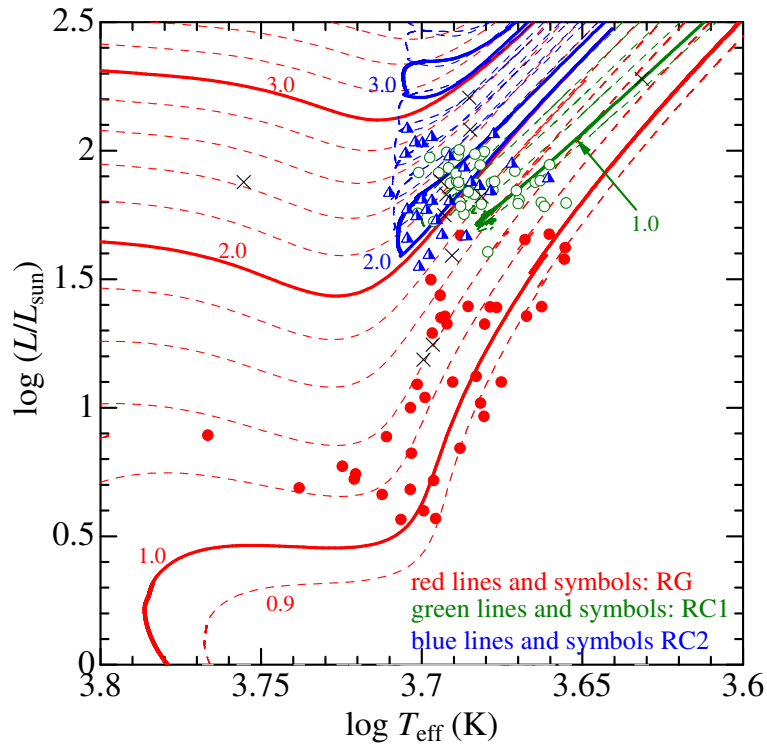


Fig. 3 The 114 program stars plotted on the $\log T_{\text{eff}} - \log L$ diagram, where the PARSEC tracks computed for $z = 0.01$ (slightly metal-deficient case by ~ 0.2 dex lower than the solar metallicity) and various M values (0.9, 1.0, 1.2, 1.4, 1.6, 2.0, 2.2, 2.4, 2.6, 2.8, 3.0, 3.2, 3.4 M_{\odot} , thick solid lines for the cases of integer masses, otherwise dashed lines) are overplotted for comparison. While 11 nearby stars are indicated simply by black crosses, the symbols for 103 *Kepler* giants are discriminated according to the evolutionary status: shell-H-burning phase before He ignition (RG) — red filled circles, $M \leq 1.8 M_{\odot}$ stars at the He-burning phase (RC1) — green open circles, and $M > 1.8 M_{\odot}$ stars at the He-burning phase (RC2) — blue half-filled triangles. Similarly, the evolutionary tracks are depicted in the relevant colours (red or green or blue) corresponding to their evolutionary stages.

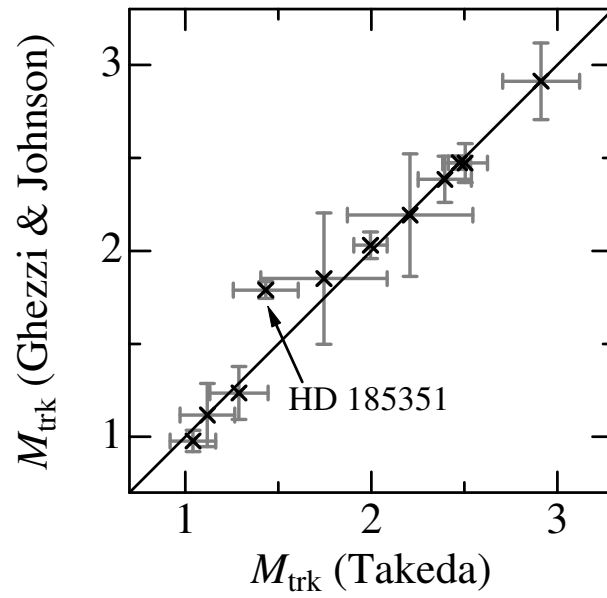


Fig. 4 Comparison of the masses derived by using PARAM in this study (abscissa) with those of Ghezzi & Johnson (2015) (ordinate) for 11 nearby giant stars in common.

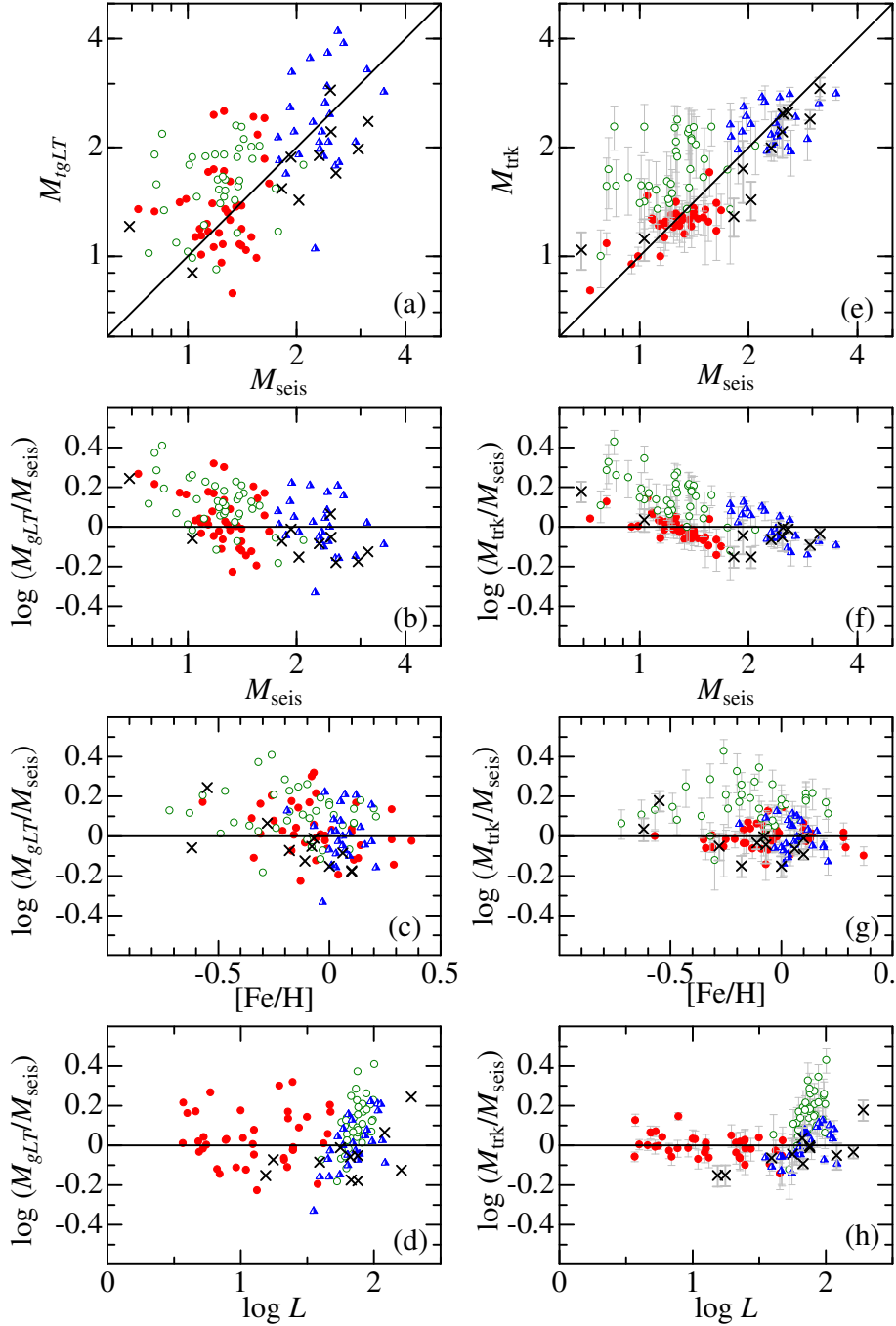


Fig. 5 Left-hand panels show how the M_{gLT} values (mass derived from g , L , and T_{eff}) of 114 program stars are compared with M_{seis} (reference mass established by the seismic technique). Comparison between M_{gLT} and M_{seis} is depicted in panel (a), while panels (b)–(d) display how $\log(M_{gLT}/M_{\text{seis}})$ correlates with M_{seis} , $[\text{Fe}/\text{H}]$, and $\log L$, respectively. Right-hand panels (e)–(h) similarly illustrate the behaviours of M_{trk} (mass derived from the position on the HR diagram by using PARAM) against M_{seis} . The meanings of the symbols are the same as in Fig. 3. Note that the axis for the mass is in the logarithmic scale.

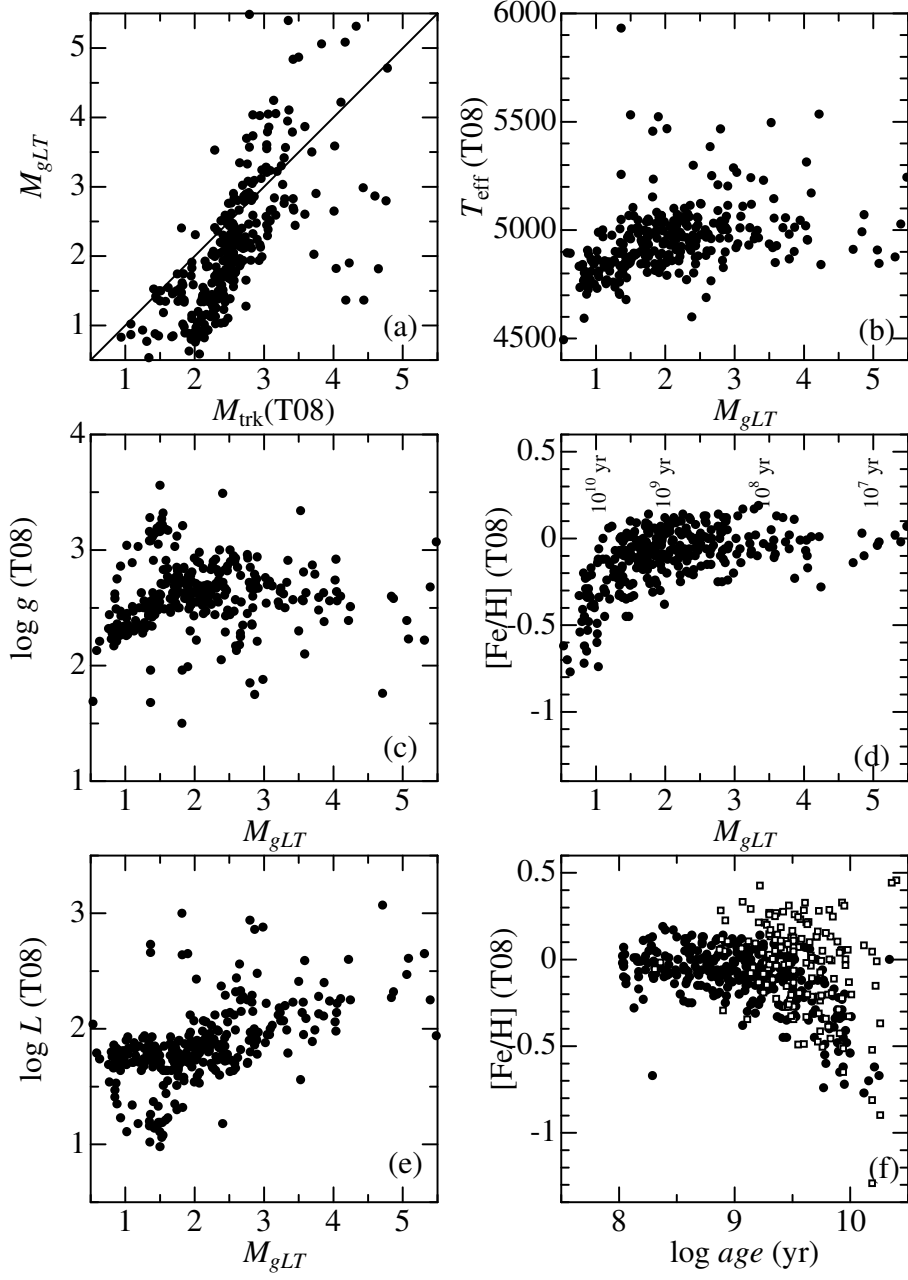


Fig. 6 Trends of the revised mass values (M_{gLT}) of 322 red giants studied in T08, which were derived from their $\log g$, $\log L$, and T_{eff} by using Eq.(1). Panel (a) shows the relation between M_{gLT} and $M_{trk}(T08)$ (derived in T08 based on theoretical evolutionary tracks), while panels (b)–(e) illustrate how T_{eff} , $\log g$, $[Fe/H]$, and $\log L$ correlate with M_{gLT} , respectively. The revised $[Fe/H]$ vs. age plots (age was derived from M_{gLT} ; cf. Sect. 5.2) are depicted in panel (f), where the age–metallicity relations for 160 FGK dwarfs (+subgiants) derived in Takeda (2007) are also overplotted in open squares for comparison.

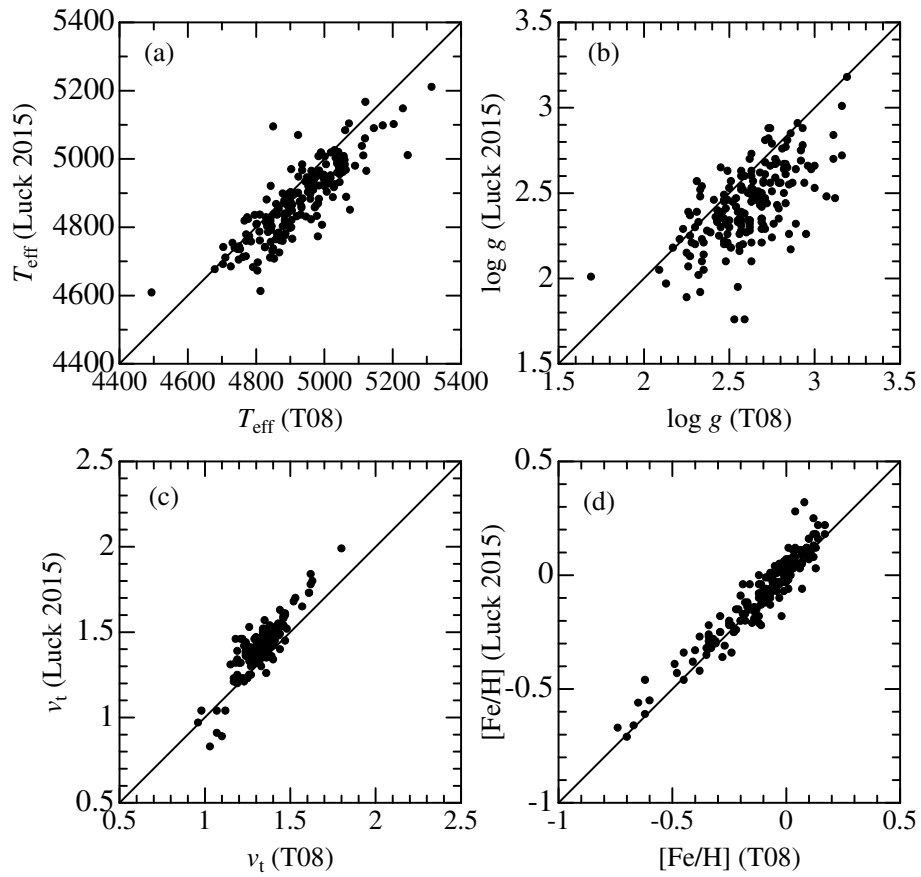


Fig. 7 Comparison of the atmospheric parameters spectroscopically determined in T08 with those derived by Luck (2015) for 189 stars in common: (a) T_{eff} , (b) $\log g$, (c) v_t (microturbulence), and (d) $[\text{Fe}/\text{H}]$.

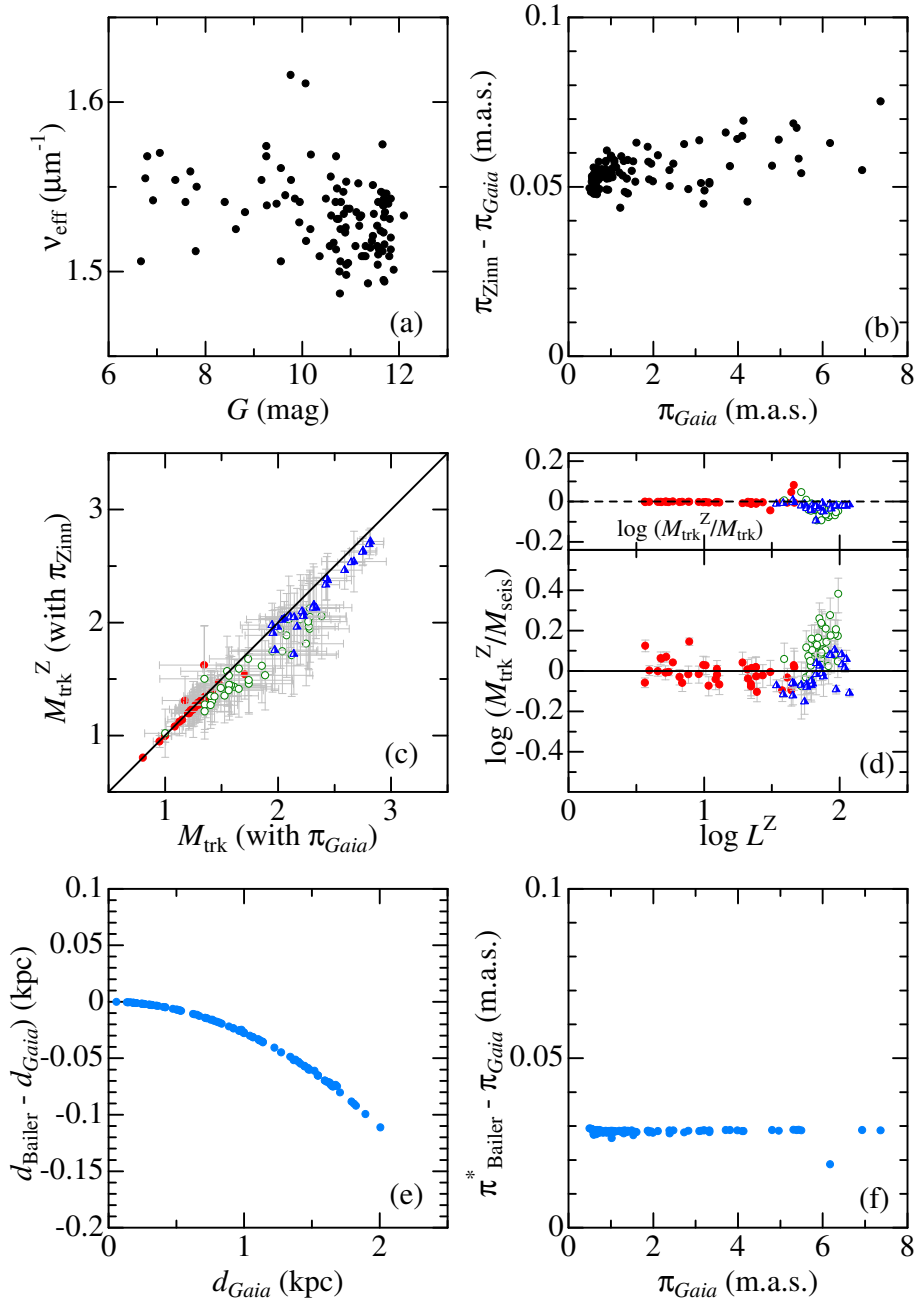


Fig. 8 (a) Correlation between G (magnitude in the G -band) and ν_{eff} (astrometric pseudocolour) for the 103 *Kepler* giants (taken from *Gaia* DR2 catalogue). (b) Zero-point offset corrections ($\pi_{\text{Zinn}} - \pi_{\text{Gaia}}$), which were evaluated from G and ν_{eff} by using Zinn et al.’s (2016) relation, plotted against π_{Gaia} . (c) Correlation between $M_{\text{trk}}^{\text{Z}}$ (derived by using PARAM but with π_{Zinn}) and π_{Gaia} -based M_{trk} derived in Sect. 4, where the meanings of the symbols are the same as in Fig. 3. (d) The logarithmic ratios of $\log(M_{\text{trk}}^{\text{Z}}/M_{\text{seis}})$ plotted against $\log L^{\text{Z}}$ (π_{Zinn} -based luminosity), which is arranged similarly to Fig. 5h for the sake of comparison. Note that $\log L^{\text{Z}}$ -dependence of $\log(M_{\text{trk}}^{\text{Z}}/M_{\text{trk}})$ is also depicted in the upper inset of this panel. (e) Distance differences for 103 *Kepler* giants between Bailer-Jones et al.’s (2018) values (d_{Bailer}) and those derived from *Gaia* DR2 parallaxes ($d_{\text{Gaia}} \equiv \pi_{\text{Gaia}}^{-1}$), plotted against d_{Gaia} . (f) Difference between the “pseudo”-parallax (formally derived as $\pi_{\text{Bailer}}^* \equiv d_{\text{Bailer}}^{-1}$) and π_{Gaia} , plotted against π_{Gaia} .